

NUCLEAR PHYSICS

DIRECT RECONSTRUCTION OF CHARMED-MESON DECAYS IN NUCLEAR COLLISIONS AT $\sqrt{s_{NN}} = 200$ GEV/NUCLEON (41 pp.)

Director of Dissertation: Spyridon Margetis

The goal of this field is the study of nuclear matter under extreme conditions of temperature and density. Such matter is believed to have existed during the first few micro-seconds of the ‘Big Bang’ that created the Universe and it might also exist in the core of a neutron star or other exotic astronomical objects. In order to re-create these conditions in the laboratory, experimentalists use large accelerators to collide nuclei of heavy elements (heavy ions, e.g. Gold, ^{197}Au) at the top energies available. It has been predicted that inside the resulting hot and dense nuclear matter the nucleon boundaries will effectively ‘melt down’ and their constituents (quarks and gluons) will be free to move over the extended interaction volume. This ‘de-confined’ phase of nuclear matter is usually referred to as ‘Quark Gluon Plasma’ (QGP), the discovery of which is our primary goal. The central issue is to identify and measure observable quantities that are sensitive to the presence of this state of matter early in the collision.

The U.S. Department of Energy funded the construction of the world’s largest heavy ion accelerator, the Relativistic Heavy Ion Collider (RHIC) at Brookhaven National Laboratory, Long Island, New York. STAR (Solenoidal Tracker At RHIC) is a multi-purpose detector aiming at measuring many different physics signals (signatures) simultaneously.

Each central, i.e. head-on, collision among two gold nuclei accelerated at RHIC is producing several thousand particles, most of them being charged and neutral pions. The detection of these particles is extremely difficult and high precision detectors combined with accurate tracking software are required. STAR has several tracking devices, i.e. detectors which record the passage of particles through different materials using their ionization properties.

One of the remaining key questions, one that will prove the QGP formation, is the question of thermalization; in order to claim the creation of a new **state** of nuclear matter one has to show sufficient degree of thermal equilibration. One of the methods that tries to probe this employs the study of particles containing very heavy quarks, the 'charm' and/or the 'bottom' quark also known as the 'beauty' quark. The idea is that if one observes that the kinetic (thermal) properties of these heavy quarks are similar to their lighter partners it will be a direct evidence of equilibrium in the system. This is because these heavy quarks are very hard to change their initial kinetic properties unless they are hit a large number of times during the lifetime of the system. Multiple collisions among a system's constituents inevitably leads to thermalization.

Up to this point no direct measurement of charm or bottom particles was possible at RHIC, but indirect methods, based on the identification of the electrons coming out of the charm and beauty decays, are used to grossly estimate their total yields.

Currently, and in preparation for future analyses, code has been developed and tested in smaller and lighter (Cu+Cu) systems. This code makes use of the enhanced pointing capabilities of the first generation silicon vertex detectors in order to allow for a statistical separation of the charm and bottom meson secondary decays (secondary

vertices) from the primary event vertex. This is what we call ‘direct’ charm-meson reconstruction. One needs to develop the appropriate tracking, vertex fitting and error propagation software, choose the best cut variables and select the cut values, in order to best optimize the signal to noise ratio.

In this thesis we develop the software tools needed to study these cut variables, their correlations and their experimental resolution. In order to do that an extensive sample of single D-meson events was generated and passed through a simulation of the full STAR apparatus in order to study the cut variable behavior in the real signal. Another simulation sample was also created containing the same signal embedded into background Au+Au events in order to study the behavior of the combinatorial background. At the same time by comparing various reconstructed quantities to the ones generated by the event generator one could study the experimental resolution of these parameters. By carefully evaluating the behavior of these cut variables for signal and combinatorial background (and also taking into account the experimental resolution), one should be able to develop a set of reconstruction cuts that maximize the signal to background ratio. The work in this thesis summarizes the first phase of this analysis, which is the thesis topic of two other Ph.D students in the group.

DIRECT RECONSTRUCTION OF CHARMED-MESON DECAYS IN NUCLEAR
COLLISIONS AT $\sqrt{s_{NN}} = 200$ GEV/NUCLEON

A thesis submitted to the
Kent State University Honors College
in partial fulfillment of the requirements
for University Honors

by

Danielle V. LaHurd

May, 2009

Thesis written by
Danielle V. LaHurd

Approved by

_____, Advisor

_____, Chair, Department of Physics

Accepted by

_____, Dean, Honors College

Table of Contents

List of Figures	v
List of Tables	vii
Acknowledgments	viii
1 Introduction	1
1.1 Introduction to Nuclear Matter	1
1.2 Quarks	2
1.3 Big Bang	3
1.4 Strong Force	4
1.5 Neutron Stars	6
1.6 Signals of Quark-Gluon Plasma Formation	7
1.7 Heavy Flavor	10
2 The STAR Experiment	13
2.1 RHIC Complex	13
2.2 STAR Detector	14
3 Simulation, Analysis, Results and Discussion	19
3.1 Event Reconstruction	19
3.2 Simulation	21
3.3 D^0 Analysis	22

3.4	Results and Discussion	24
3.4.1	Invariant Mass and Kaon Decay Angle in COM system	25
3.4.2	Reconstructed decay vertex and its resolution	32
3.4.3	Transverse Momentum p_T	34
4	Summary	40
	References	41

List of Figures

1.1	An example of a baryon and a meson. The baryon includes three quarks of three colors, while the Meson contains a quark and anti-quark of a color and anticolor.	3
1.2	Diagram of a neutron star showing layers of matter types.	8
1.3	Phase diagram of nuclear matter	9
1.4	Higgs quark mass vs. total quark mass (i.e. naked mass vs. dressed mass)	12
2.1	Various facilities for accelerating ions at RHIC.	14
2.2	Perspective view of STAR experimental apparatus	15
3.1	The reconstructed invariant mass distribution of simulated D^0 decays.	25
3.2	Shown here is a schematic of the decay of the D^0 into its daughters. In the lower left is shown the center of mass frame. This figure represents some variables used in cuts.	26
3.3	Center of mass Kaon decay $\cos \theta$ in D^0 decays.	27
3.4	Center of mass Kaon decay $\cos \theta$ versus reconstructed invariant mass in D^0 decays.	28
3.5	Graph of the $\cos \theta$ versus the reconstructed transverse momentum of the kaon. The blue/red points correspond to low/high momentum D^0 decays.	30
3.6	Graph of the $\cos \theta$ versus the transverse momentum from both the Kaon and the parent D^0 particles.	31

3.7	The center of mass decay angle for both signal and background versus the reconstructed mass of the decay. The area in the oval shows the $\text{Cos } \theta$ around the signal mass of $1.86 \text{ GeV}/c^2$	33
3.8	The decay vertex X position versus the reconstructed X position. Units are in centimeters.	34
3.9	The resolution of the x axis. Units are in centimeters.	35
3.10	The decay vertex Y position versus the reconstructed Y position. Units are in centimeters.	36
3.11	The differences between the reconstructed and GEANT Z position of the decay vertex versus the Z vertex from GEANT. Units are in centimeters.	37
3.12	The percentage resolution of the $D^0 p_T$ fitted with a Gaussian curve (pink). The y-axis depicts the number of counts at the percentage. . .	38

List of Tables

1.1	Table of quark flavors, charges, and masses. For understanding the mass a proton has a mass of about 1 GeV.	2
-----	---	---

Acknowledgments

I would like to thank my research advisor, Dr. Spyridon Margetis for everything he has done. His support and advice in this thesis and everything else has been invaluable. I would also like to thank Joe Vanfossen for putting up with my rambling and answering the stupid questions that came to mind. Questions that I really should have known the answer to had I calmed down to think about them.

I would like to thank everyone on my defense committee. I know you did not have to take that time out of your busy schedule.

Chapter 1

Introduction

The purpose of the RHIC facility and the experiments housed there, such as STAR, is to study nuclear matter (i.e. strongly interacting, or QCD, matter) and its properties in extreme conditions of temperature and pressure in order to gain insight about the origin of our universe but most importantly to test a fundamental prediction of QCD, the theory of strong interaction, that at high temperatures and/or nuclear densities, quarks and gluons should form a weakly coupled parton plasma (soup).

1.1 Introduction to Nuclear Matter

Ordinary matter contains an atomic nucleus, and its electron shell. Nuclear matter, however, is comprised entirely of nucleons, the components of atomic nuclei. Since an atom's mass resides 99.9% in its nucleus, this gives nuclear matter a density far greater than ordinary matter. The density of ground state, pure nuclear matter can be calculated to be about 10^{14} more dense than normal matter.

The calculation is simple: Take the assumption that there are 0.2 nucleons per cubic femtometer(fm). Multiply this number by the mass of a nucleon (2×10^{-27} kg) and you get $\rho_{nuclear} = (0.2 \text{ nucleon}/\text{fm}^3)(2 \times 10^{-27} \text{ kg}/\text{nucleon}) = 4 \times 10^{11} \text{ kg}/\text{cm}^3$

As an example, it is estimated that a spoonful of pure nuclear matter weighs as much as all the water in Lake Erie. Such a state of matter could be found in objects such as neutron stars. Nucleons themselves are composite particles. As they are baryons, they are made up of combinations of three quarks, combinations of the up

Quark name	Symbol	Charge	Approximate Mass(GeV/c ²)
<i>Up</i>	u	+2/3	0.005
<i>Down</i>	d	-1/3	0.01
<i>Strange</i>	s	-1/3	0.2
<i>Charm</i>	c	+2/3	1.5
<i>Top</i>	t	+2/3	180
<i>Bottom</i>	b	-1/3	4.7

Table 1.1: Table of quark flavors, charges, and masses. For understanding the mass a proton has a mass of about 1 GeV.

and down quark. Up/Down is called flavor of the quark.

1.2 Quarks

Quarks have spin of $1/2$ integers, like all fermions, and carry a charge of either $1/3$ or $2/3$. Protons are made from two up quarks, charge $+2/3$ and one down quark, charge of $-1/3$, for a total charge of $+1$. Neutrons are made from two down quarks and an up quark ($-1/3 + -1/3 + 2/3$), with a total charge of 0 .

Quarks have two additional degrees of freedom, flavor and color. Quarks come in six flavors: up, down, strange, charm, bottom, and top. Table 1.1 shows the quark flavors and their attributes. Baryons are made of three quarks, while mesons are made from a quark anti-quark pair, $q\bar{q}$. The other degree of freedom is color. Color is a name for the strong or nuclear force, i.e. only colored objects (objects carrying a color charge) are allowed to interact strongly. The mediator of the strong force is the gluon, a spin 1, mass less, field boson. There are three varieties of color: red, green, and blue. Ordinary matter is colorless; therefore colors must cancel once the quarks form baryons or mesons. A combination of the three colors or three anti-colors will result in a 'colorless' particle. Therefore, a baryon made of three quarks and an anti-baryon made of three anti-quarks will be colorless, as all three colors are represented with the

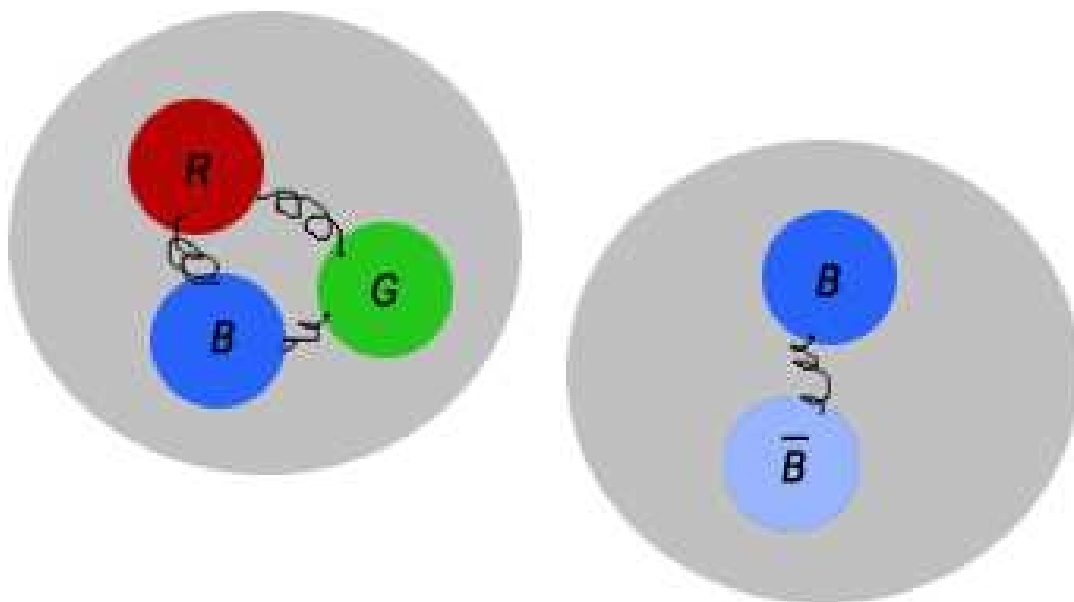


Figure 1.1: An example of a baryon and a meson. The baryon includes three quarks of three colors, while the Meson contains a quark and anti-quark of a color and anticolor.

quarks. Mesons, too, must be colorless. Since they are made of only two quarks, the three-color combination to create a 'colorless' particle will not work. Instead, mesons form from a quark and an anti-quark, one color and one anti-color. The color and anti-color cancel each other out leaving the colorless meson. The theory of the strong force between color charges is called quantum chromodynamics (QCD).

1.3 Big Bang

Most theories suggest the universe began with a 'big bang', a large outward explosion of space, time, and energy. The first few microseconds of this explosion were full of extreme conditions and exotic matter as the temperature allowed for particles to form out of the infant universe. The temperature of these first moments was trillions of degrees ($T > 10^{12}\text{K}$). Quarks, gluons and other basic forms of matter such as

electrons and neutrinos existed freely.[1]

Particle accelerators, through particle collisions, reproduce these extreme temperatures, simulating the first few microseconds of the big bang. We can reproduce these 'mini bangs' as often as necessary to study the phenomena that may have occurred as the universe was born. This will give us greater understanding of the world around us and how it was formed.

1.4 Strong Force

The strong force is one of the four fundamental forces, along with the electromagnetic, the gravitational, and the weak forces. It, like other forces, has a force carrier, the gluon. Gluons are unlike photons as a force carrier in that they *do* have color charge as well as carry it, while photons cannot have an electric charge. This allows gluons the ability to decay or interact with other gluons, while photons cannot decay into other photons. This feature of gluons makes the strong force potential unlike all the other forces to increase with distance. The strong force remains constant with distance (up to a certain distance away) while the other three forces are inversely proportional to distance squared ($\propto 1/r^2$). Due to the strong force or color force, we cannot view individual quarks by pulling them apart. By trying to separate the quarks, the work done or the energy required for further separation increases. After a certain point, the energy to separate the two quarks is enough to form a quark anti-quark pair according to Einstein's equation $E = mc^2$. This being more energetically favorable than further separation, the quarks then 'snap back', never leaving a confined state of either a baryon or a meson.

Quark confinement can be explained another way, via the MIT Bag Model. In simplistic terms, quarks and gluons are inside a 'bag', which represents the baryon or

meson. Inside this 'bag' mass of the quarks is zero, but, outside the bag, this mass reaches infinity. The quarks, therefore, cannot escape the bag as they do not have the energy, and remain confined.

In order to view individual quarks we must take a different route. By colliding two heavy nuclei together at near relativistic velocities, we compress and heat the matter. This heat produces many new particles while they are still confined in a very small space.

For example, a typical particle has a radius of 0.7 fm. Gold, the heavy nuclei collided at RHIC, have a radius of

$$R_{Au} = 1.12A^{1/3} = 6.5 fm$$

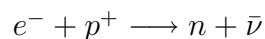
When collided, the two Au nuclei form a rough cylinder shape of roughly $154 fm^3$. With every particle having a radius of .7 fm and on the order of thousands of particles packed within that volume, there is nowhere near enough space to contain them all. Soon, there is no way to tell which quarks belong to which particles in the gigantic mass. This mass then becomes a 'soup' of quarks. This soup forms what is called the Quark Gluon Plasma (QGP). A plasma is an overall neutral state (roughly equal numbers of positive and negative charges), where the charges are not bound to one another.

We consider this QGP a new state of nuclear matter, due to it being in thermodynamic equilibrium. We use the thermodynamic terms because the system is very large, many thousands of particles interacting. These individual collisions take less time than the single large collision of the two gold nuclei. The small collisions reach equilibrium before the system expands.

1.5 Neutron Stars

Neutron stars are formed when stars above 1.4 solar masses, above the Chandrasekhar limit, reach the end of their life cycle. These stars have fused all of their hydrogen and have begun fusing heavier elements in their cores. These elements fuse into heavier elements up to iron, where fusing no longer grants any energy. When fusing no longer grants energy, the outward pressure holding the star up under its own mass falls. As the fusion pressure fails, the electrons degenerate pressure, the pressure of the electrons resisting as they are squeezed closer together due to the Pauli Exclusion Principle, builds up. At a certain point this pressure becomes greater than the mass pushing inward and the star explodes outwards in a supernova.

If the core of the star survives, with the core's mass between 1.5 and 3 times the mass of the sun, it will collapse back into itself. The electron pressure cannot hold this mass up just like before the supernova. The electrons merge with the protons in a process called inverse beta decay forming a neutron and an anti-neutrino.



This process forms the two particles into a dense hot sphere of neutrons, which also have a degeneracy pressure. The degeneracy pressure of neutrons is greater than that of electrons and can support the mass of a star less than about 5 solar masses. Should the mass be greater, the force of the collapse would overcome even this pressure, forcing the mass into a point and creating a black hole.

A neutron star, like all stars, is made up of layers. It has a thick outer crust, followed by an inner crust, outer core, and inner core. The inner and outer crusts are made of regular matter, such as electrons, protons and neutrons. The outer core is made of dense nuclear matter. However, in the deepest reaches of the neutron

star, the pressure is so great that the Pauli Exclusion Principle may not hold up for even the neutrons. Since the neutrons are packed so closely together, the quarks and gluons may become de-confined as described in a previous section forming a QGP at the heart of the neutron star.

Some theories also claim that there are stars made entirely of strange matter (that is matter that contains strange quarks) called quark stars. These hypothetical stars would follow the same cycle as the neutron stars, but the remnants would be on the heavier limit. The collapse would be more than the neutron star but not enough for a full collapse into a black hole.

Figure 1.3 shows the relation of heat and density of nuclear matter, and shows where neutron stars and experiments such as RHIC fall on the scale.

1.6 Signals of Quark-Gluon Plasma Formation

In order to find signals of the QGP we could look at the emitted photons from the collision. The photons emitted are black body radiation, providing information on the temperature from the collision. However these photons are difficult to detect due to many particles decaying into π^0 particles. The π^0 particle decays into two photons, therefore trying to find the few black body photons in a sea of millions of π^0 photons is a daunting task.

Another method of probing is examining the strangeness of matter (i.e. strange quarks) coming from the collision. By looking at the amount of strange quarks we gain some insight on the QGP. Strange quarks take more energy to form than the up and down quarks that comprise regular matter.

One other way is the presence of heavy flavored matter. Charmed quarks have a high mass and a relatively small cross section, making them sensitive probes for

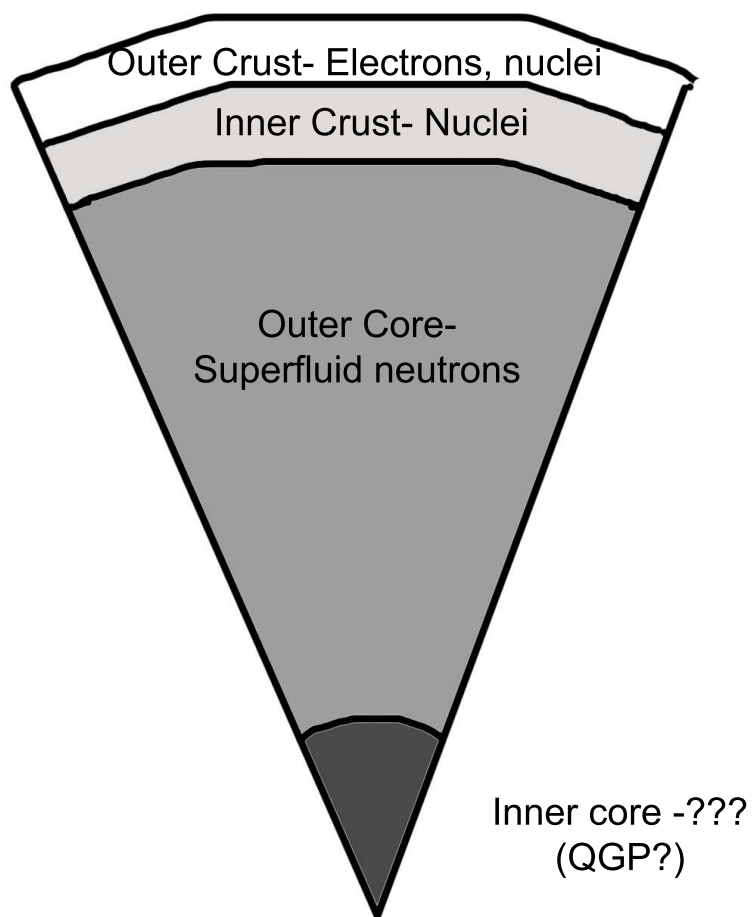


Figure 1.2: Diagram of a neutron star showing layers of matter types.

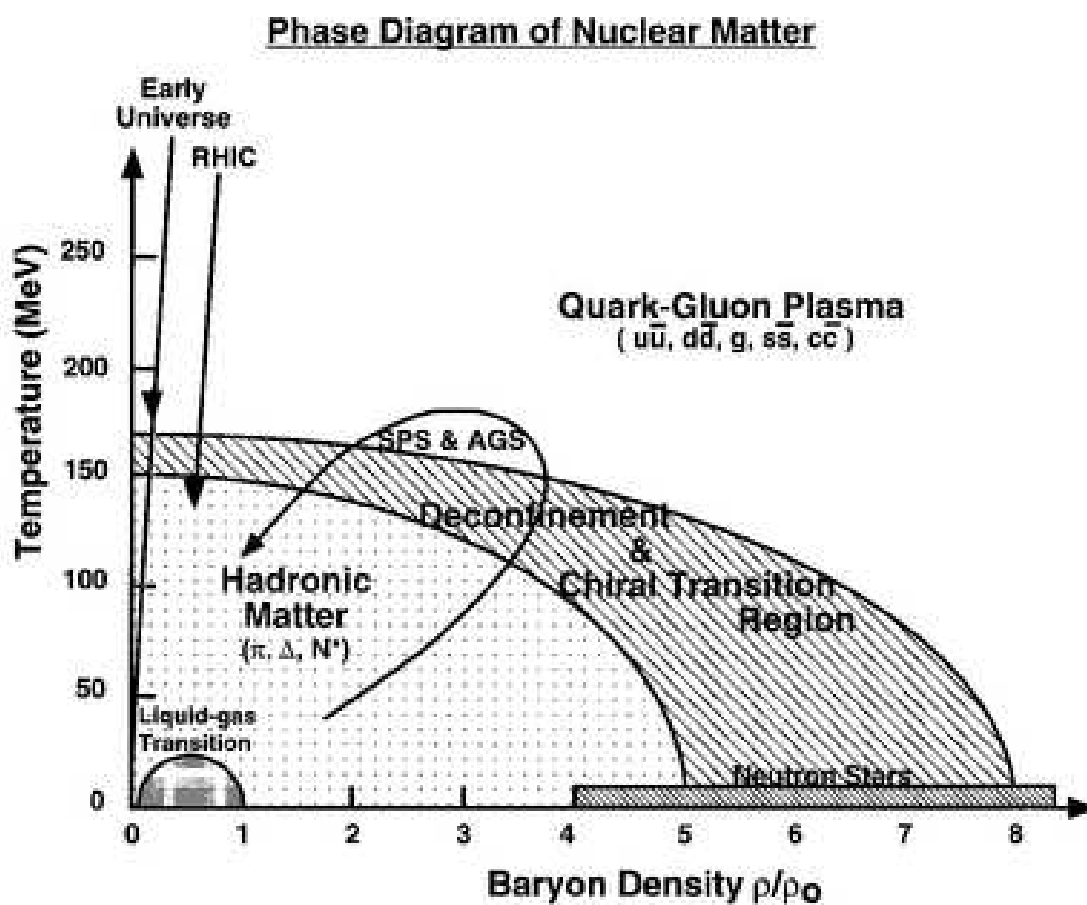


Figure 1.3: Phase diagram of nuclear matter

the frequency of interaction and the degree of thermalization. We will discuss this in more depth in the next section.

1.7 Heavy Flavor

Heavy flavor matter is matter containing one of the heavy quarks, quarks above the mass of the strange quark. (See Table 1.1 for list of masses.) The heavy quarks are the charm, bottom and top quarks. These quarks require a great deal of energy to produce due to their heavy masses ($E = mc^2$), and are produced through gluon fusion or $q\bar{q}$ annihilation during the initial phase of the interaction because only then is the full kinetic energy available. These quarks therefore can only form very early in the collision, nearly the initial state of the collision. The total yield of the heavy quarks presents information about the initial stage of the collision. Heavy quarks should also provide insight into the dynamics of the initial collision.

Charmed hadron flow is an indication of thermalization due to the interaction of light quarks and gluons on the heavy quarks. If quarks in heavy hadrons flow in the same pattern as those in light hadrons, it is an indicator of many collisions between all quarks (thus thermalization). If we find out that the data supports the flow of heavy quarks then this is going to be the smoking gun of thermalization i.e. the formation of QGP.

Up and down quarks have bare masses of a few MeV, but in protons three of them add together to produce a mass of 1GeV, therefore their dynamical mass is about 300 MeV. Split three ways, this makes the individual quarks in the nucleon orders of magnitude more massive than their naked counterparts. Heavy quarks on the other hand are not as influenced by the QCD vacuum as the light quarks (up, down, strange). This can be seen in Figure 1.4. The heavy quarks, charm, bottom

and top, lie on the 1:1 ratio between the Higgs vacuum and the QCD vacuum. The lighter quarks fall below that line, demonstrating the differences between their Higgs mass and their QCD mass. This feature makes the heavy flavor a very useful tool because their naked (Higgs) and dynamical (QCD) mass are almost identical.

Heavy quarks have kinematically suppressed gluon radiation while passing through a medium, implying that the heavy quarks should lose less energy in denser media. However, current measurements indicate the energy loss for these quarks is unexpectedly high, meaning the theory for heavy quark energy loss may be wrong.

Direct measurements of the heavy flavor hadrons produced are not possible due to the short half-lives of the particles, therefore other methods must be used to study these particles.[2] Also current detectors cannot differentiate between the D-mesons, those with a charm quark, and the B-mesons, those with a bottom quark. Since the mass, and therefore the time of production, of the mesons is different, it would be beneficial to know the difference between the two.

The mass of the D^0 meson is 1.865 GeV, and is comprised of a charm and anti-up quark. The mass of a B^0 -meson is just under 3 times the mass of the D^0 -meson and is comprised of a down and anti-bottom quark. We shall be focusing on the analysis of the D^0 -meson and its daughter particles, most specifically the decay of:

$D^0 \longrightarrow K^- + \pi^+$ that occurs in 3.89% of all D^0 s produced. Since it is common, and both daughter particles have charge, it is easy to detect.

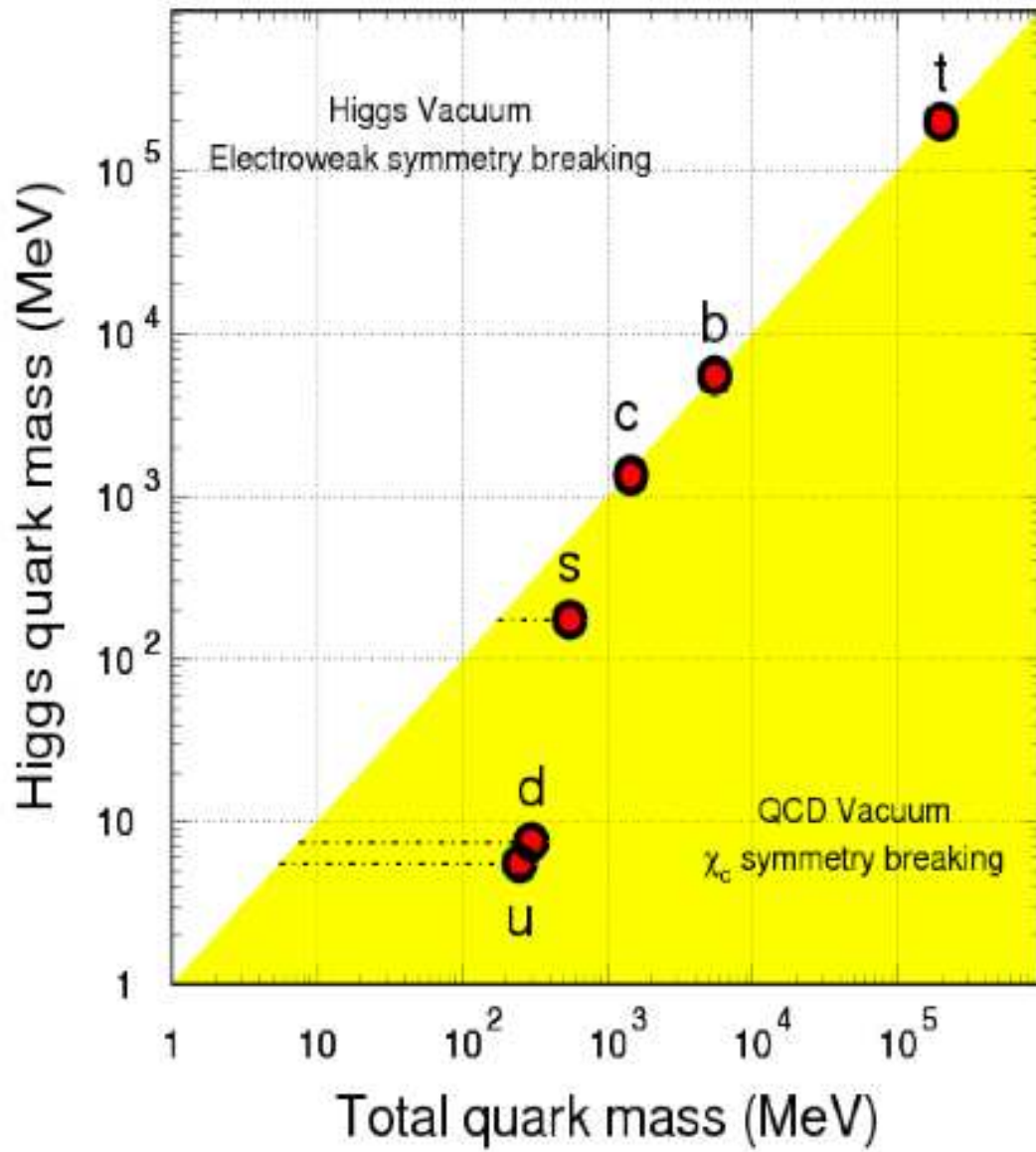


Figure 1.4: Higgs quark mass vs. total quark mass (i.e. naked mass vs. dressed mass)

Chapter 2

The STAR Experiment

The Solenoidal Tracker at RHIC (STAR) is one of the four main experiments run at the Relativistic Heavy Ion Collider (RHIC). STAR and PHENIX are the two largest experiments being conducted at present, and are at 6 o'clock and 8 o'clock respectively on the RHIC ring. The other two experiments, PHOBOS and BRAHMS, were at 10 o'clock and 2 o'clock but they are now decommissioned. There are an additional two collision points on the ring at 12 and 4 o'clock. The objective of RHIC is the discovery of QGP.

2.1 RHIC Complex

RHIC began its operation in 2000 at Brookhaven National Lab (BNL) in Upton, New York. In order to accelerate the heavy ions for the experiments, the ions must go through several stages in the facility to accelerate them to relativistic speeds. The most important equipment in this process are the Tandem Van de Graff, the Booster synchrotron, the Alternating Gradient Synchrotron (AGS) and the RHIC ring itself. A diagram of these apparatuses is seen in Figure 2.1

The ions are placed into the Tandem Van de Graff, which uses static electricity to accelerate and remove electrons from the exterior of the ions. The ions are then sent to the Tandem-to-Booster line which carries them to the Booster synchrotron. At the Booster, a circular accelerator, the ions are accelerated even more through the use of electromagnetic waves. The Booster sends the ions towards the AGS for further

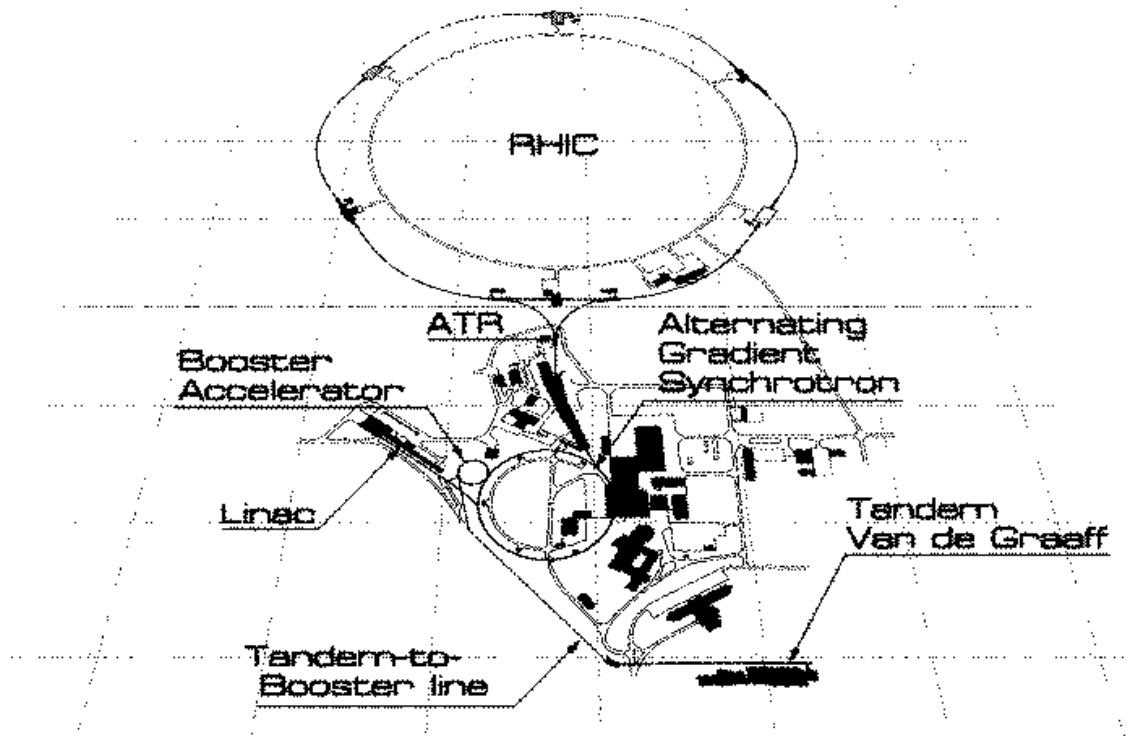


Figure 2.1: Various facilities for accelerating ions at RHIC.

acceleration after bringing their speed to $0.37c$. At the top acceleration from the AGS, the ions are then transferred by the AGS-to-RHIC line which sends them into one of the two RHIC rings (clockwise and counter-clockwise) for collision. At the RHIC ring, the ions are boosted to $0.997c$, their top relativistic velocity, and stripped of their last remaining electrons. The collision points are occupied by various experiments, such as STAR, located near the insertion point (i.e. 6 o'clock), and PHENIX. [3]

2.2 STAR Detector

The STAR detector was designed to measure hadron production over a large solid angle. STAR has complete azimuthal symmetry and a pseudorapidity η range of $-1.3 < \eta < 2$. This large acceptance lends itself well to hadron jet detection and

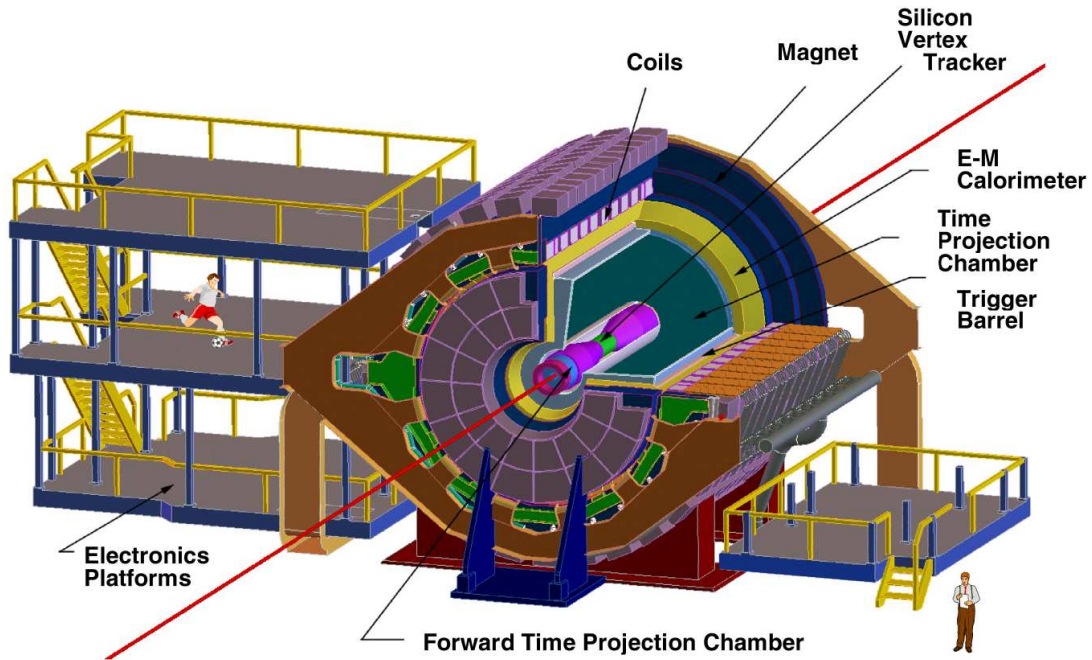


Figure 2.2: Perspective view of STAR experimental apparatus

single event characterization of ion collisions. (Pseudorapidity relates with the polar angle of the emission so that when the particle is emitted normal to the beam the pseudorapidity goes to zero. When the particle emission direction approaches the direction of the beam, η goes to $\pm\infty$.) The main components of the apparatus are the Magnet, the Triggers and Data Acquisition (DAQ), the Time Projection Chamber (TPC) and the Silicon Vertex Tracker (SVT)

The main feature of the STAR apparatus is the Time Projection Chamber (TPC) that lies within the bulk of the detector. For the TPC to work properly and detect the momentum of the particles traveling through it, a strong and uniform magnetic field is required. The field in the STAR apparatus is along the z-direction and has an operating range of $0.25 < |B_z| < 0.5T$ (nominal value) with excellent uniformity.

The entire assembly weighs over 1100 tons, and provides support for most other

components of the detector. Deflections in the magnet structure are minimized to less than 1 mm to preserve magnetic field quality. The coils in the star magnet are constructed from hollow rectangular aluminum insulated with fiberglass and vacuum impregnated with epoxy. At the field maximum (0.5 T) the main coils draw a current of 4500 A. The coils are cooled by a closed loop water cooling system with a flow rate at 1200 gallons per minute. The cooling system dissipates 3.5 MW to keep coils at an operating temperature of 29°C . [4]

Due to the fast event rates compared to the slow readout time of the Time Projection Chamber, STAR requires the use of a multi-level trigger system to process and select events. STAR has four trigger levels, L0, (L1, L2), L3. There are two stages of trigger levels. L0, (L1, L2) are the fast triggers and read out at every beam crossing (every 105 ns). These trigger levels receive information on the multiplicity and global energy of the collisions, and select events accordingly. L3 is the second stage trigger and receives information from the tracking detectors. STAR has three primary fast triggers: Central Trigger Barrel (CTB), Zero Degree Calorimeter (ZDC), and Barrel Electromagnetic Calorimeter (BEMC).

STAR has multiple triggers leading into the Data Acquisition (DAQ). The main task of the DAQ system is to read the data input from the STAR detectors, a rate of 20,000 MB/sec, to reduce that rate to 30 MB/sec and store it. This large input rate demands parallel processing in the DAQ system, which at the end writes about 100 events/second on tape. (The DAQ has since been updated to 1000 events/second.) [5]

The Time Projection Chamber (TPC) is the central detector for STAR. It is the central element in the detectors around the vertex of interaction. The TPC must have

the ability to track and identify particles over the widest range possible, with complete coverage along the beam-line. The TPC provides complete tracking for particles with up to ± 1.8 units of pseudorapidity and can record particles with momenta greater than 100MeV. The TPC at STAR is the largest in the world as of 2003 and has dimensions 4m in diameter by 4.2m long.

The TPC identifies particles by measuring ionization energy loss (dE/dx) as well as records tracks and momenta. It is filled with P10 gas (10% methane, 90% argon) holding a uniform, well defined, electric field. The gas is kept at 2mbars of pressure. The electric field is approximately 135 V/cm. The paths of the particles are reconstructed through the secondary electrons in the gas released at the particles passing that drift towards the readout end caps, located at the ends of the chamber. The electric field is defined by a conductive membrane located at the center of the TPC and other connecting devices such as the connecting end caps. The tracks are reconstructed with high precision, below a millimeter in deviation. The electric field uniformity is critical due to the long drift paths of the electrons and extreme precision.

TPC reconstructs the primary path of a particle by finding ionization clusters along the track separately in the x, y and z space (with the z -axis along the beam line). [6]

The Silicon Vertex Tracker (SVT) is located at mid-rapidity near the beam line. It is a three barrel microvertex detector based on silicon drift detector technology. The main purpose of the SVT is to enhance the physics capabilities in the TPC. The SVT improves upon the primary vertexing, two track separation resolution and energy loss measurement used in particle identification. The SVT allows for reconstruction of very

short-lived particles, potentially including the D-mesons (charmed mesons), using secondary vertexing close to the interaction point. It also increases the kinematical acceptance for particles with low momentum, using the SVT alone as some particles fail to reach the detectors in the TPC due to the magnetic field.

The SVT is made of 216 silicon drift detectors (SDD) which are solid state time projection chambers. The SDD are made from N-type silicon wafers with a thickness of $280\mu\text{m}$. Cathode strips are placed on top and bottom of the wafers biased towards the drift direction. Anodes are placed on the edge of the detector, parallel to the cathode strips. Electrons generated by an ionized particle passing by, drift towards the middle of the detector, then towards the anodes. The SSD provide unambiguous two dimensional hit position measurements and contain over 13 million pixels. (A pixel is defined by an anode segment in one coordinate and the drift velocity divided by the sampling frequency in the drift direction.)

Position resolution is of $20\mu\text{m}$ in both coordinate directions with the SVT at STAR, and the energy loss resolution was about 7%. [7]

Chapter 3

Simulation, Analysis, Results and Discussion

3.1 Event Reconstruction

While STAR collects an enormous amount of data, full reconstruction of the collision events must occur before detailed physics analysis can be performed. The reconstruction process is similar for the TPC and the SVT (and other detectors on STAR), differing in track density, detector orientation or readout capacity. We will briefly discuss the reconstruction process for the TPC.

The trajectory of the particle is reconstructed by finding ionization **clusters**. The ionization clusters are produced from secondary electrons, formed by the collisions of a charged particle with the electrons of gas atoms. The hits, where the electrons or charged particles have crossed a TPC pad row, correspond to the trajectory. The clusters are found on a two dimensional coordinate system, the X-Z plane, defined by the TPC pad row and drift directions. Clusters are found where adjacent hits exist on the X-Z plane and may indicate one or more particles. For hit finding, the clusters must be deconvoluted (in the case of hit overlap) into their individual hits then the center of the hit is found based on the charge distribution.

Global tracking is the process of taking the reconstructed hits and combining them into tracks that represent the path of the charged particle through the detector. To begin this process, a seed, a short series of hits close to each other, must be found for the track. Seeds are most efficiently found in low hit density regions, often in the outer padrows of a sector. Once a segment is found, tracking software merges

close together segments under the assumption they are likely from the same particle, eliminating split tracks where multiple tracks are reconstructed for the same particle. The final step in global tracking is to refine the fit parameters taking into account loss of energy and multiple scattering between hits.

The **primary vertex** is the main interaction point where the collision occurred. Secondary vertexes can form from particle decays or other isolated processes. The primary vertex is found by using the reconstructed global tracks and extrapolating them to the beam line. The main bin along the beam line (Z direction) is then chosen as the seed for the primary vertex.

After finding the seed, the Distance of Closest Approach (DCA) of each global track is calculated with respect to the primary vertex seed. Tracks found with a DCA greater than a set distance are eliminated and the total DCA is minimized in order to refine the vertex candidate.

Tracks assumed to originate from the interaction point are refined once the primary vertex is found by including that location in the fit. The refit is neglected for tracks with DCA greater than 3cm from the vertex and is refined. Tracks that improve their quality measure with the inclusion of the primary vertex are kept, while those that diminish are removed.

Particles can be **identified** through their energy loss as they pass through the TPC. The energy loss depends on the particle's velocity and is reflected by the amount of ionization it causes. By knowing the momentum, from tracking, the dE/dx can be plotted as a function of the particles momentum. Particles with the same momentum will show on the plot due to different masses and therefore different velocities. [8]

3.2 Simulation

STAR simulation software is a powerful tool allowing for full simulation of Au-Au collisions and the STAR response to the collision. Simulating events allows for the exact lifespan and yield of particles to be reproduced perfectly thus allowing for limited geometrical acceptance corrections. Simulations also allow for embedding of standard candles, a track of a known particle, into a raw event, in order to estimate the apparatus' reconstruction efficiency. Also the simulation environment allows for testing of newly developed analysis software through use of these standard candles.

STAR simulation tools are of three categories, event generators, material simulators and detector response simulators. The event generators simulate a collision event including all particles produced during the ion collision. The material simulator reproduces the effect the detector material has on the particles produced in the collision. Lastly the detector response simulators mimic how the detectors, such as the TPC, respond to the particles, i.e. they incorporate the detector resolutions.

HIJING (Heavy Ion Jet Interaction Generator) is a Monte Carlo event generator developed by M. Gyulassy and X.N. Wang, used in the study of high velocity ion collisions. It was designed to simulate the jets and particle production produced from proton-proton (pp), proton-nucleus (pA), or nucleus-nucleus (AA) collisions. HIJING is based on QCD interaction models and complies with data from high energy and heavy ion experiments. The program reproduces spectra including two particle correlations and can explain the average momentum dependence on multiplicity and observed flavor. [9]

The GEANT program simulates the passage of particles through matter and was first designed for high energy physics experiments. The program now has two main

applications: 1) tracking particles through a setup for detector response simulation and 2) graphical depiction of particle trajectories and experimental setup. As an example, GEANT can simulate multiple scattering, including Coulomb and hadronic, and the energy loss due to ionization. [10]

The TPC Response Simulator (TRS) is the STAR software used to simulate the response of the TPC to the passage of particles. The TRS takes over from GEANT once the trajectories are known. The output of this program is equivalent to an actual output from the STAR TPC and may be sent to reconstruction software for tracking, hit, and cluster finding.

Data returning from reconstruction holds more information than raw data from an event. The reconstructed data contains all the information of the Monte Carlo event originally and is used to compare the input particles with the reconstructed tracks. The hits of the Monte Carlo particle are known. If the reconstructed track has the same number of hits as a simulated track, the two tracks are "associated".

Monte Carlo events are simulated ion collisions made in HIJING and passed through the analysis chain of GEANT, TRS, and the association maker.

Embedding allows for an environment as close to a real STAR event as possible. Monte Carlo tracks are embedded into actual STAR raw events. This is useful if one wants a comparison of particles and reconstructed tracks as close to a real STAR event as possible. The embedding process has further uses in studying geometrical acceptance and reconstruction efficiency.

3.3 D^0 Analysis

MuKpi ($\mu K\pi$) is the D^0 analysis and reconstruction program. It is used to determine if D^0 -mesons were produced in an event through looping several times on the

stored event structure. During the loops, quality cuts are made over the number of TPC fit hits, p_T , pseudorapidity η , and loss of energy track length. The cuts are applied on both the positive and negative daughters from the D^0 decay, K^- , π^+ . Once both tracks are found we calculate, among other things:

- 1) The decay length
- 2) The invariant mass defined as: $M_{inv}^2 = M_+^2 + M_-^2 + 2(E_+E_- - p_+^z p_-^z)$

The matching of the GEANT with the reconstructed events from *MuKpi* is a multi-step process and in this initial run all events reconstructed in either GEANT or *MuKpi* are simulated. First the events are run over with the *MuKpi* macro to collect the reconstructed D^0 s. The same event files are then run over with GEANT to get the D^0 information. The comparison required the writing of a C++ macro to run over the data contained within the two files, GEANT and *MuKpi*, compare specific values for matches and then save the variables from these matches into a separate file called a tree or ntuple. Analysis of the variables was completed in the ROOT environment.

Searching for a specific signal in a set of thousands or more is a difficult task. During an event, millions of particles and tracks are created. In order to find the D^0 s we need to eliminate some of this background noise and enhance the signals of the D^0 s specifically. In order to achieve this we perform a series of cuts and eliminations based on the parameters of the particle and the background.

One method of singling out the D^0 s is to eliminate the background as much as possible. By doing this we are eliminating some of the D^0 output, but we are also gaining a great deal of reduction in the surrounding noise. In order to make this cut, we must compare the D^0 only events to $D^0 +$ HIJING events, which include the

background behavior.

Background subtraction can only eliminate so much of the background from the data depending on the simulation software used. Analysis cuts are used to further eliminate background signal and preserve the D^0 signal. Cuts may enhance the signal far more than a background subtraction, eliminating the background by up to 90%.

3.4 Results and Discussion

Our goal is to use the simulated D^0 files and the D^0 plus HIJING files to study the behavior of the various kinematical and geometrical variables. These variables are also known as cut variables due to the ability to cut the extent of their data range in order to examine certain events in more detail but more importantly to suppress the background. The actual value of any cut is limited by its resolution, a value that must be determined. For example, you cannot cut on a variable $v < 0.005$ if your resolution is 0.5 since you will throw away most of your signal. From the D^0 only files, we can acquire information on the behavior and resolution of the cut variables in the signal. Using the $D^0 + \text{HIJING}$ files, we can acquire information about the background data. Through the background data, and its resulting behavior, we can then further refine the cut variables. In the end, we need two items from the simulated data for the signal and background. From the signal, we require the cut variable distributions and their resolution of the D^0 only events. We also require the same cut variable distribution for the background HIJING event. The following discussion is the initial analysis in this direction. This analysis is going to be followed up until the complete behavior of the chosen cut set is well understood in its every aspect. By optimizing the cut-variable space one hopes to optimize the Signal/Background ratio thus minimizing the measurement's statistical errors.

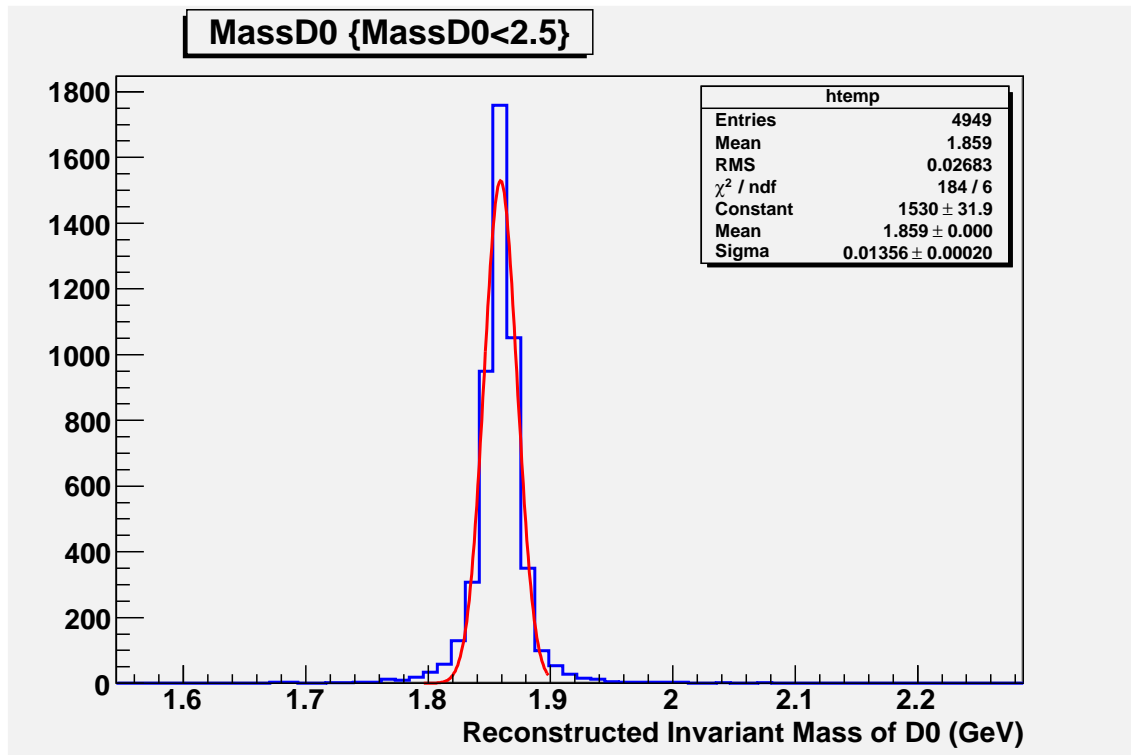


Figure 3.1: The reconstructed invariant mass distribution of simulated D^0 decays.

3.4.1 Invariant Mass and Kaon Decay Angle in COM system

Invariant Mass

The reconstructed invariant mass of D^0 decays are shown in figure 3.1. Since the simulation uses the exact mass value for the D^0 , which is 1.865 GeV the plot shows the actual experimental resolution. We see that the mean reconstructed value of 1.859 GeV is less than 1% away from the actual value. This indicates that the tracking and the reconstruction code are bug free. The fitted (with a Gaussian curve) sigma is 13.6 MeV which is 0.7 % of the mass and it is compatible with the momentum resolution of the experiment. This initial and most fundamental check of the reconstruction code (which is newly developed and used for the first time) gives us the confidence that the basic functionality of the program is sound.

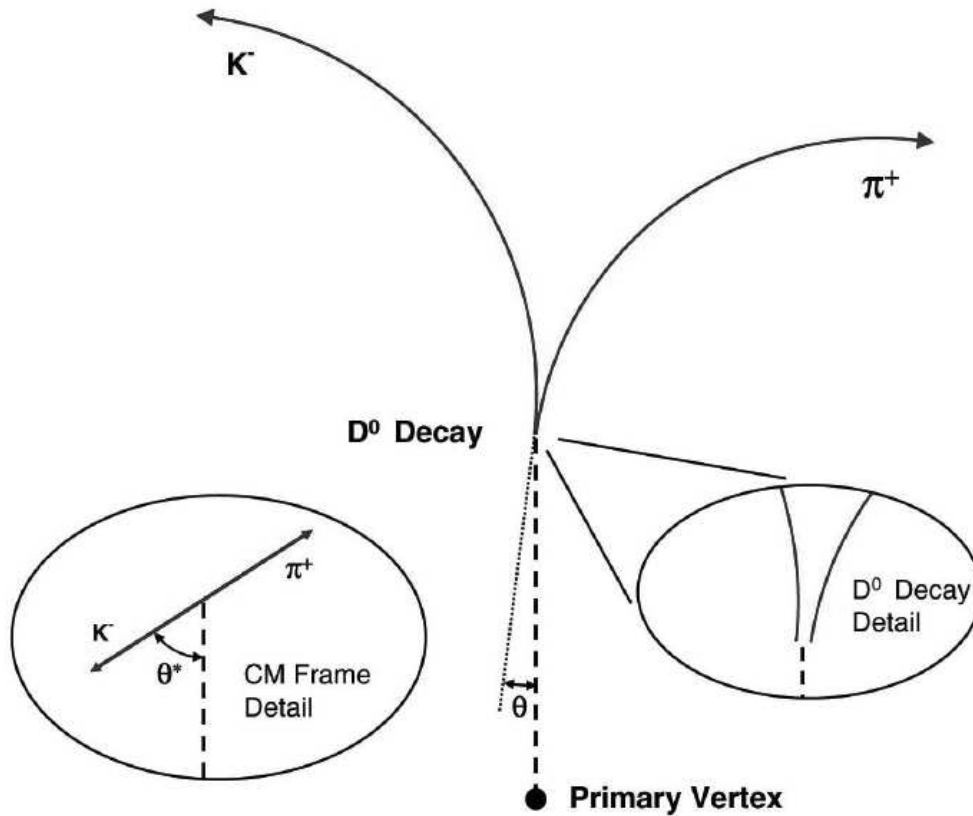


Figure 3.2: Shown here is a schematic of the decay of the D^0 into its daughters. In the lower left is shown the center of mass frame. This figure represents some variables used in cuts.

Kaon decay angle in the D^0 rest frame

The two decay particles in the rest frame of the D^0 are flying back to back. The decay process should be uniform in all directions in that frame, therefore uniform in ϕ , the azimuthal angle, and $\cos\theta$, the polar angle, due to the presence of the $\sin\theta$ term in the solid angle, i.e. $\sin\theta d\theta = d\cos\theta$. A reference to this decay can be seen in Figure 3.2. The picture in the lower left of the figure depicts the decay in the COM (Center Of Mass) frame. The variable θ^* refers to the angle between the kaon decay in the COM frame and the direction of the D^0 momentum in the lab frame.

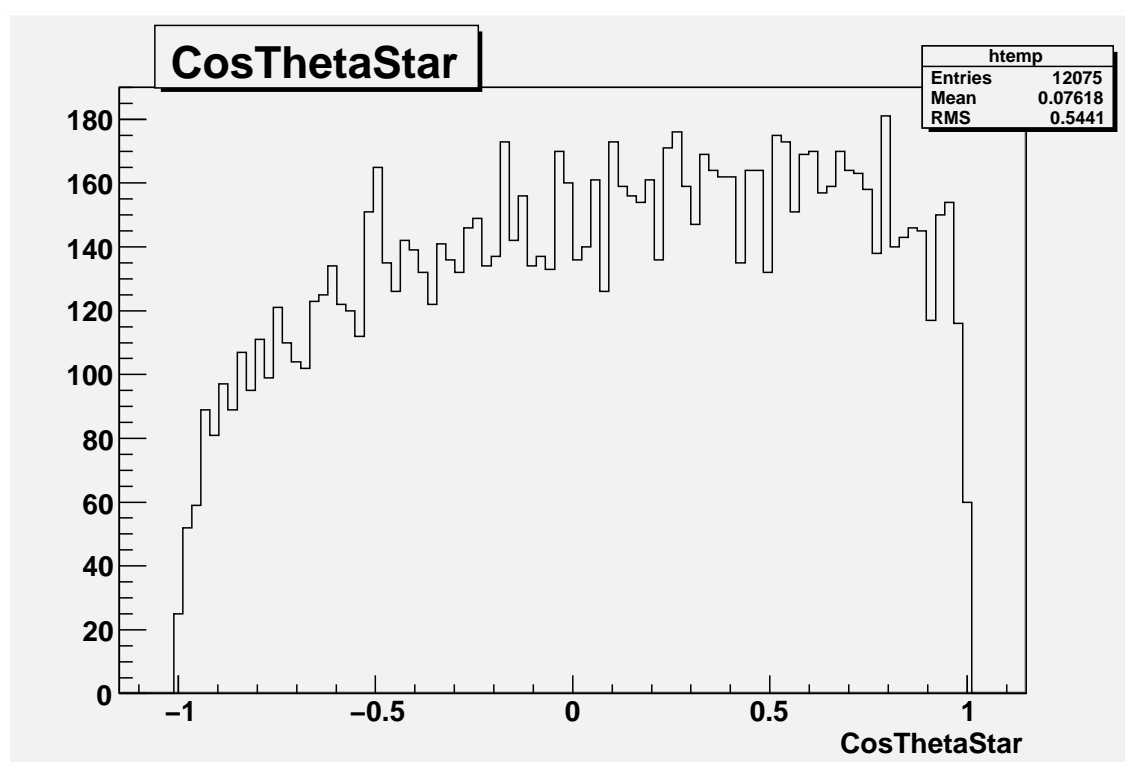


Figure 3.3: Center of mass Kaon decay $\cos \theta$ in D^0 decays.

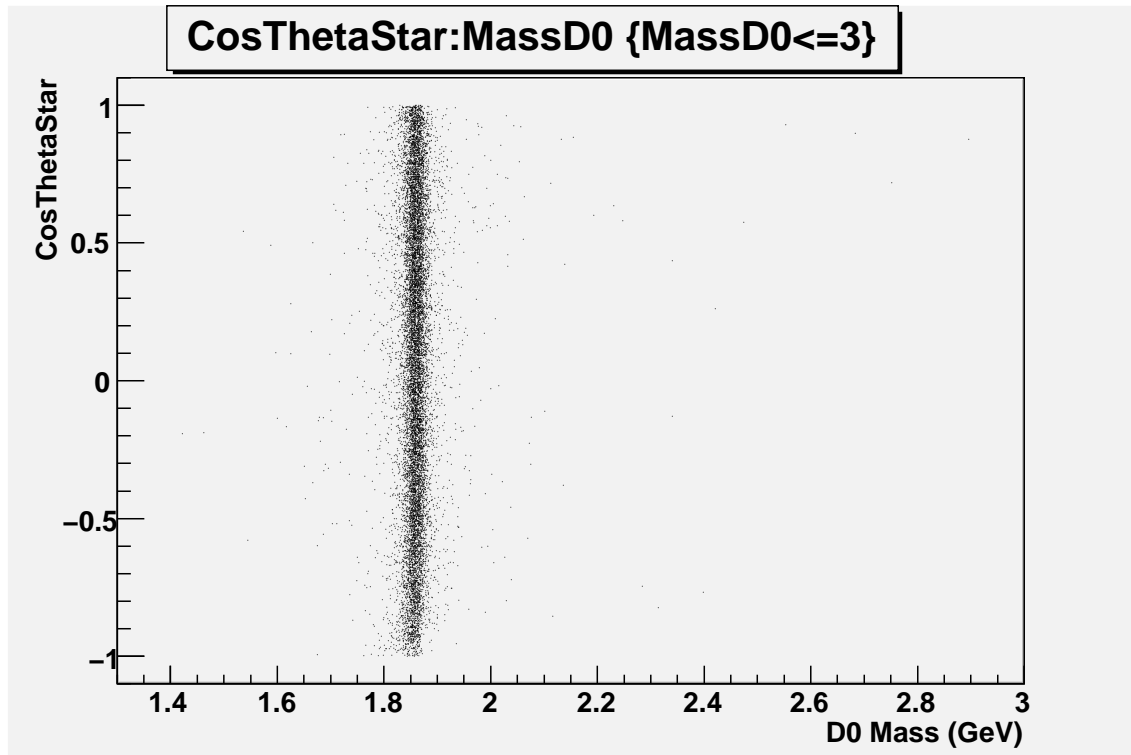


Figure 3.4: Center of mass Kaon decay $\cos \theta$ versus reconstructed invariant mass in D^0 decays.

The cosine of the center-of-mass decay angle for a sample of D^0 decays is shown in figure 3.3, and we notice that it is not flat as expected but it shows a depletion at large negative values. The reason for this depletion could be either a bug in the reconstruction code or a kinematical fact. In either case we decided to investigate further. These decays come from the K^- particles having a cosine of near -1, that is a 180° orientation from the D^0 direction.

In figure 3.4 we show the COM kaon decay angle versus the reconstructed invariant mass. We see no big correlation of the depletion with the mass but there is a slight hint of the mass turning towards lower values at large negative cosine values. Actually, it is hard to notice the depletion itself in this scatter plot. We decided to look at

momentum correlations of the decay angle for the following reason. The kaon is emitted in the opposite direction from the D^0 direction. Also, there is no significant Lorentz boost to daughter particles since we are in a collider environment, not fixed target and the COM coincides with the Lab frame. Actually, since the D^0 is very heavy, the boost factor ($\beta\gamma$) is about 0.5 for a D^0 with the average p_T (about 1 GeV). A slow kaon in the opposite direction is going to be even slower after the 'boost' in the opposite direction. The track reconstruction efficiency of the TPC has a very steep slope at low momenta, therefore these soft kaons are likely not to be reconstructed, something that logically would explain the depletion. To check this hypothesis we plotted the decay angle versus the laboratory p_T of the kaon and this is shown in figure 3.5.

There are two data sets on the graph in Figure 3.5:

- 1) The blue data set corresponds to the values where $p_{TD^0} < 2$ GeV.
- 2) The red data set corresponds to the values where $p_{TD^0} > 2$ GeV.

We immediately notice that for large negative values of the decay angle the kaons are very soft as opposed to high angle values where the mean p_T is above 1 GeV. Our hypothesis is correct; the depletion at large negative angles comes from pure kinematic reasons coupled to a strong dependence of the reconstruction efficiency to particle momentum for low momenta.

To further demonstrate this kinematical reason we plotted the decay angle versus both the parent and kaon transverse momentum. This is shown in figure 3.6. For large negative cosines both the p_T of the kaon and/or the D^0 congregate towards very low values thereby giving less efficient reconstruction probability. The lesson we learn from this is that we should avoid the extreme values of decay angles since in either

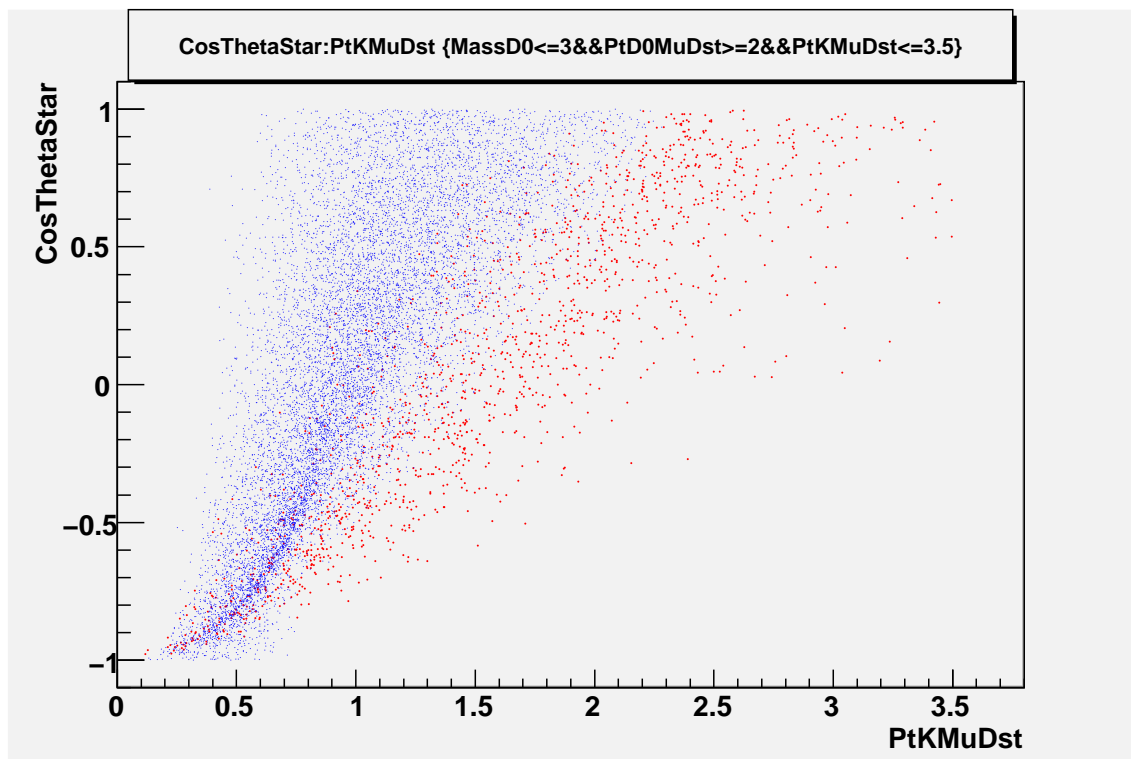


Figure 3.5: Graph of the $\cos \theta$ versus the reconstructed transverse momentum of the kaon. The blue/red points correspond to low/high momentum D^0 decays.

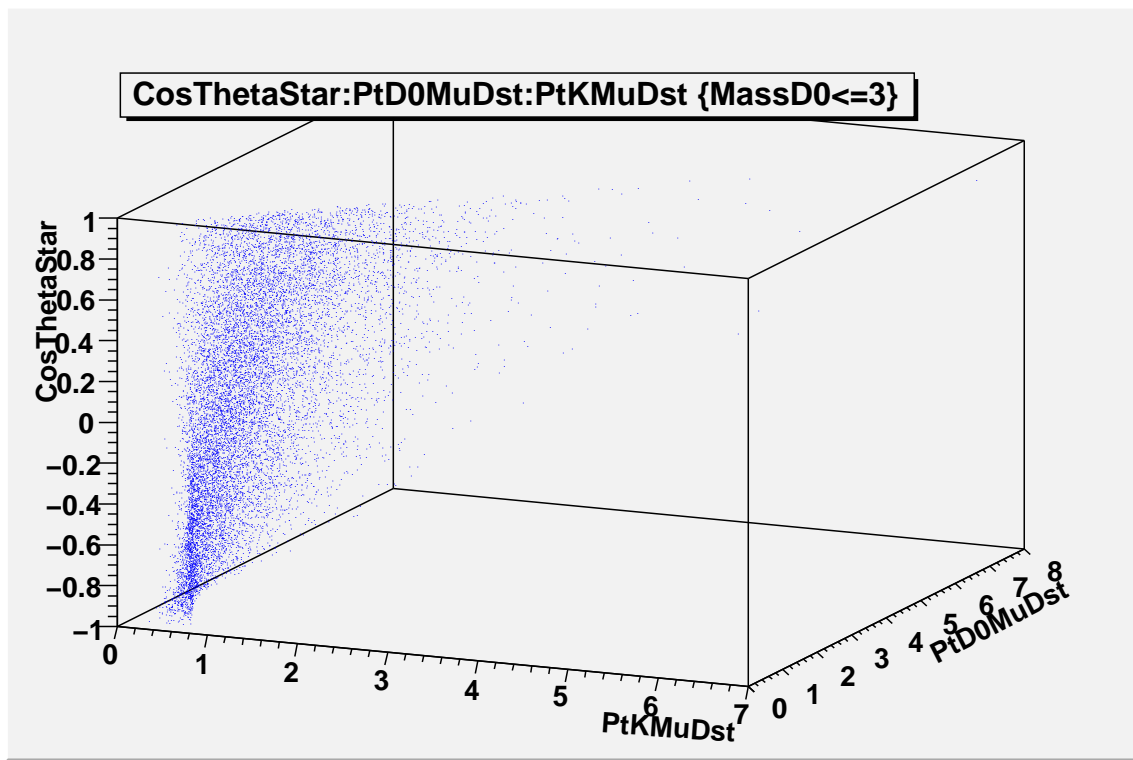


Figure 3.6: Graph of the $\cos \theta$ versus the transverse momentum from both the Kaon and the parent D^0 particles.

case (low or high) one of the decay products is going to be very soft, therefore poorly reconstructed and of low overall quality.

The next step is to look at the behavior of the background and study possible correlations that will allow us to further optimize this decay angle cut.

Figure 3.7 shows the decay angle versus the reconstructed invariant mass but for both D^0 meson decays and the background. The oval indicates the region where the mass is around the expected (real) mass of 1.86 GeV. A line is clearly seen, as expected, for the D^0 signal; the rest is background. We see that around the expected mass the background is limited; most of it is actually concentrated around the extreme values of the decay angle. Remember that these are the areas that the previous study told us to eliminate. Therefore by choosing, e.g. cosine theta values between -0.5 to 0.5 we get rid of most of the background and also get away from areas that are not kinematically favorable.

3.4.2 Reconstructed decay vertex and its resolution

We turn now to study the decay vertex characteristics. Figures 3.8 and 3.10 show the GEANT versus the reconstructed position of the D^0 decay vertex, the X and Y transverse coordinate correspondingly, in centimeters. We notice that most of the decays are within 200 microns from the event vertex. We also observe a correlation which is diagonal with a certain width. This means that the reconstruction code does a good job within its experimental resolution parameters. It is hard to 'read' by eye the width of the correlation but it looks like it is around 100 microns, a crude estimate of the resolution. In a further analysis of the X vertex resolution, seen in Figure 3.9, we find that the central peak, shown with a double Gaussian fit in red, has a width of about 100 microns. However, this fitting demonstrates the peak has

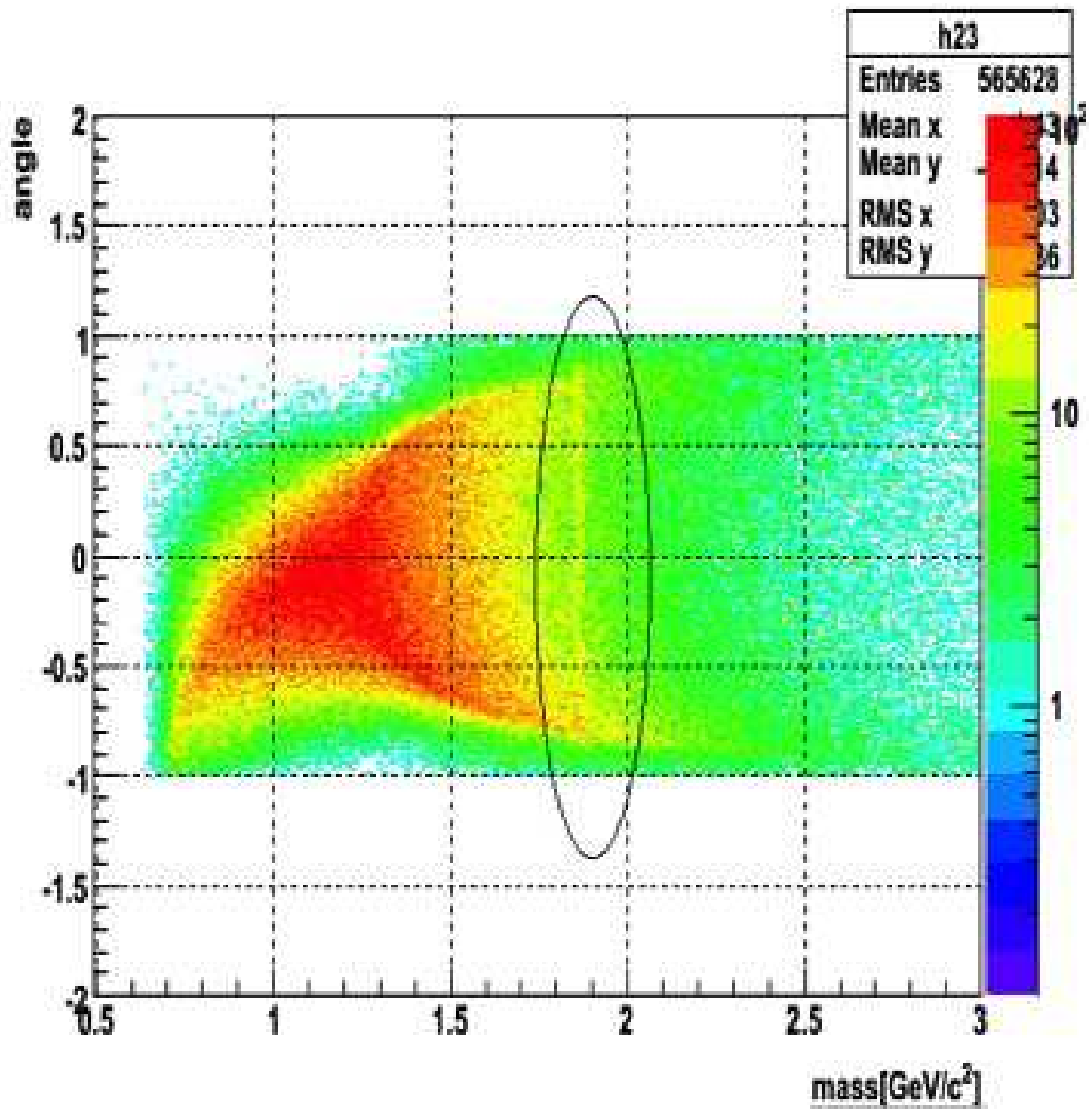


Figure 3.7: The center of mass decay angle for both signal and background versus the reconstructed mass of the decay. The area in the oval shows the $\text{Cos } \theta$ around the signal mass of $1.86 \text{ GeV}/c^2$.

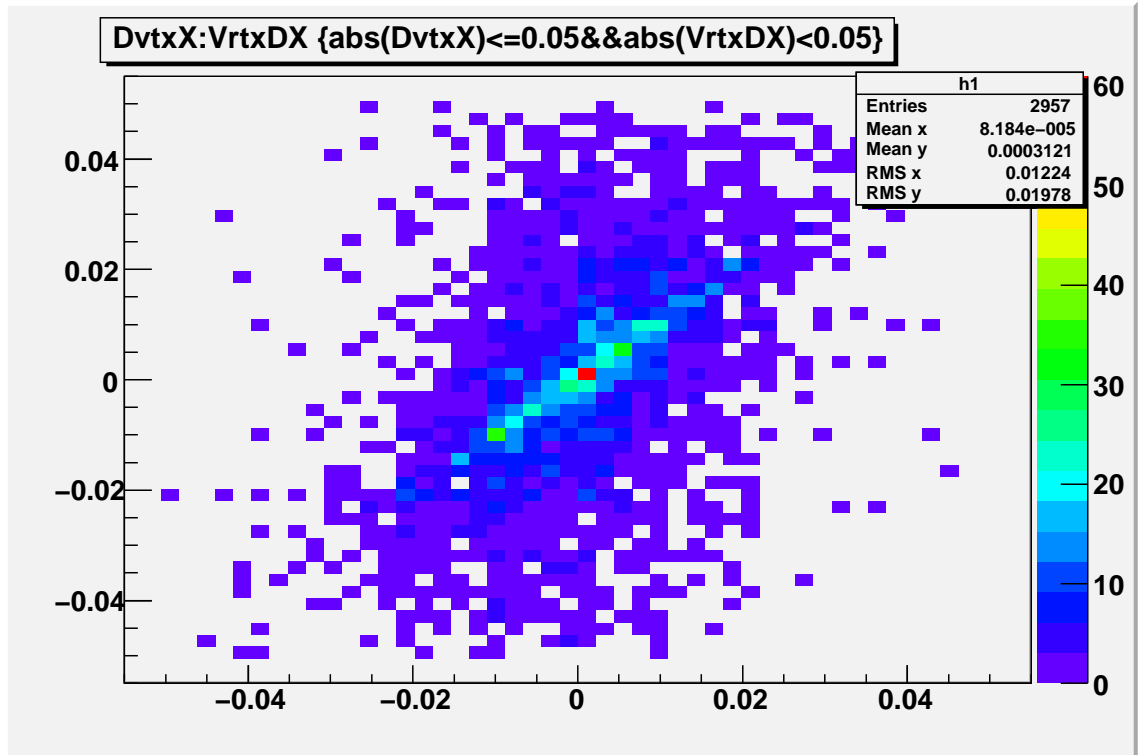


Figure 3.8: The decay vertex X position versus the reconstructed X position. Units are in centimeters.

strong non-Gaussian tails.

In order to quantify the resolution and also study possible position dependent effect we should plot the difference (Rec-MC) versus the MC value and perform a width analysis. We demonstrate this with the following graph in figure 3.11 where we show the third coordinate, Z , which is the beam direction. A more detailed analysis of such correlation will follow in the future.

3.4.3 Transverse Momentum p_T

Figure 3.12 shows the percentage resolution of the D^0 transverse momentum variable. We observe that the mean is well centered at zero (no biases). We fitted the

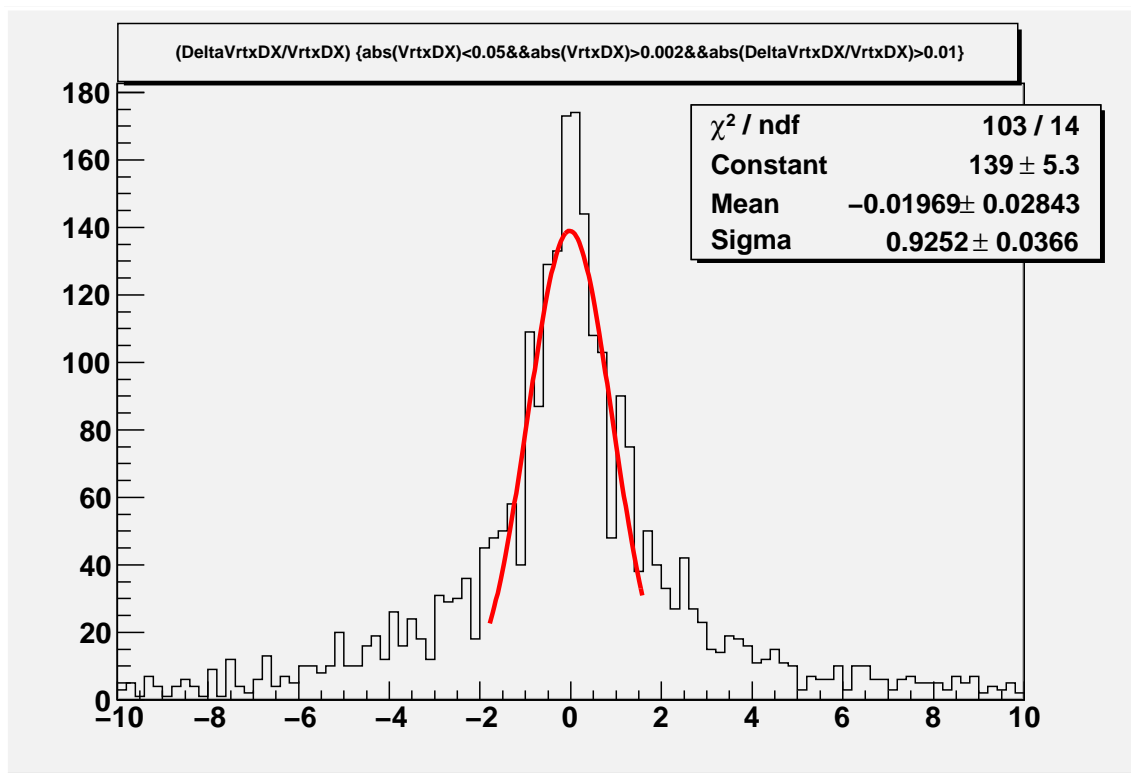


Figure 3.9: The resolution of the x axis. Units are in centimeters.

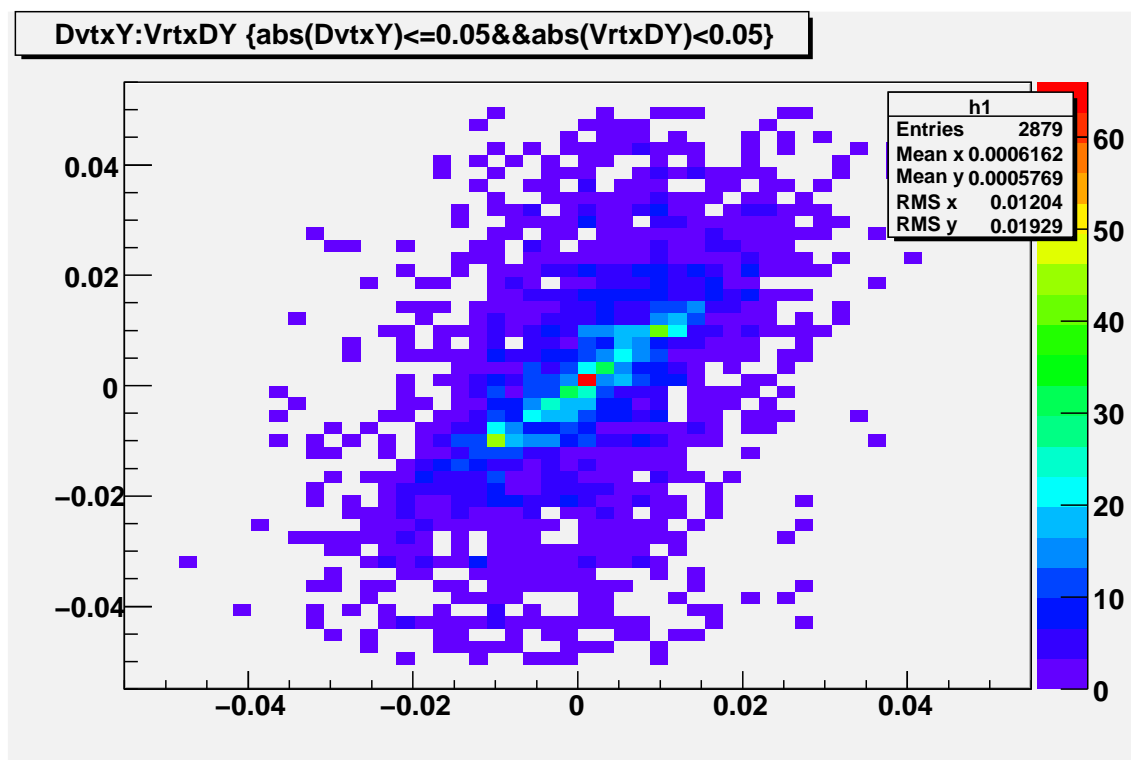


Figure 3.10: The decay vertex Y position versus the reconstructed Y position. Units are in centimeters.

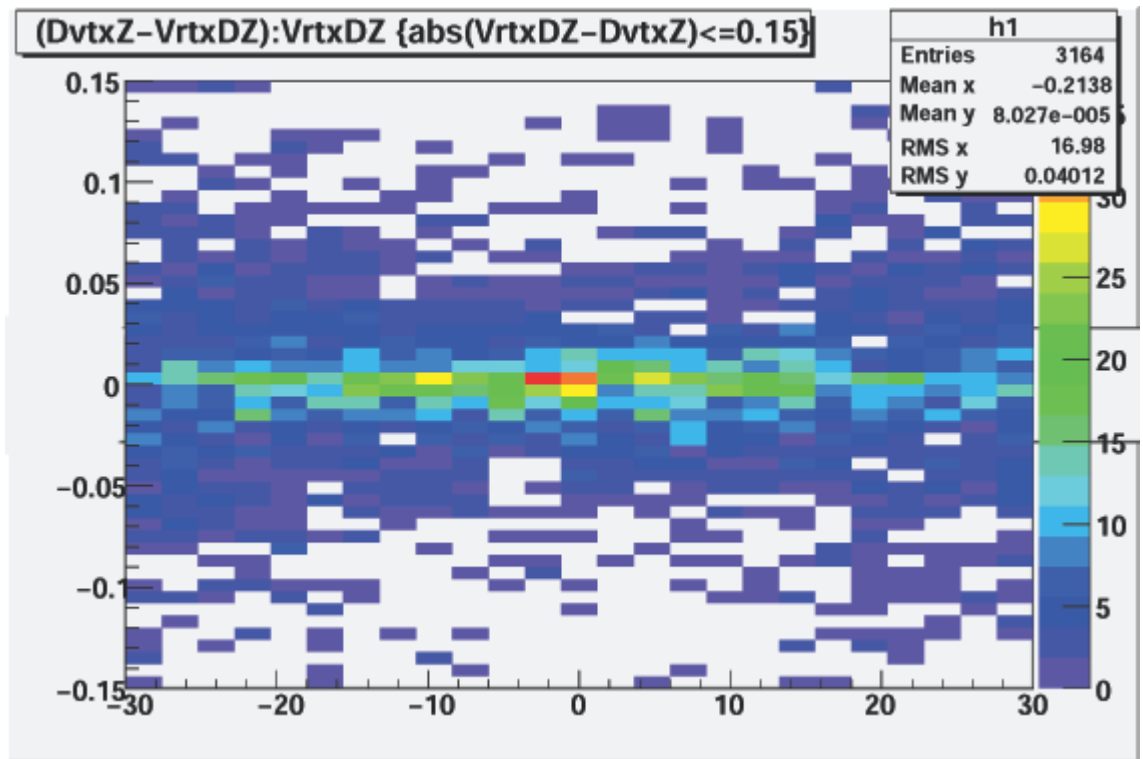


Figure 3.11: The differences between the reconstructed and GEANT Z position of the decay vertex versus the Z vertex from GEANT. Units are in centimeters.

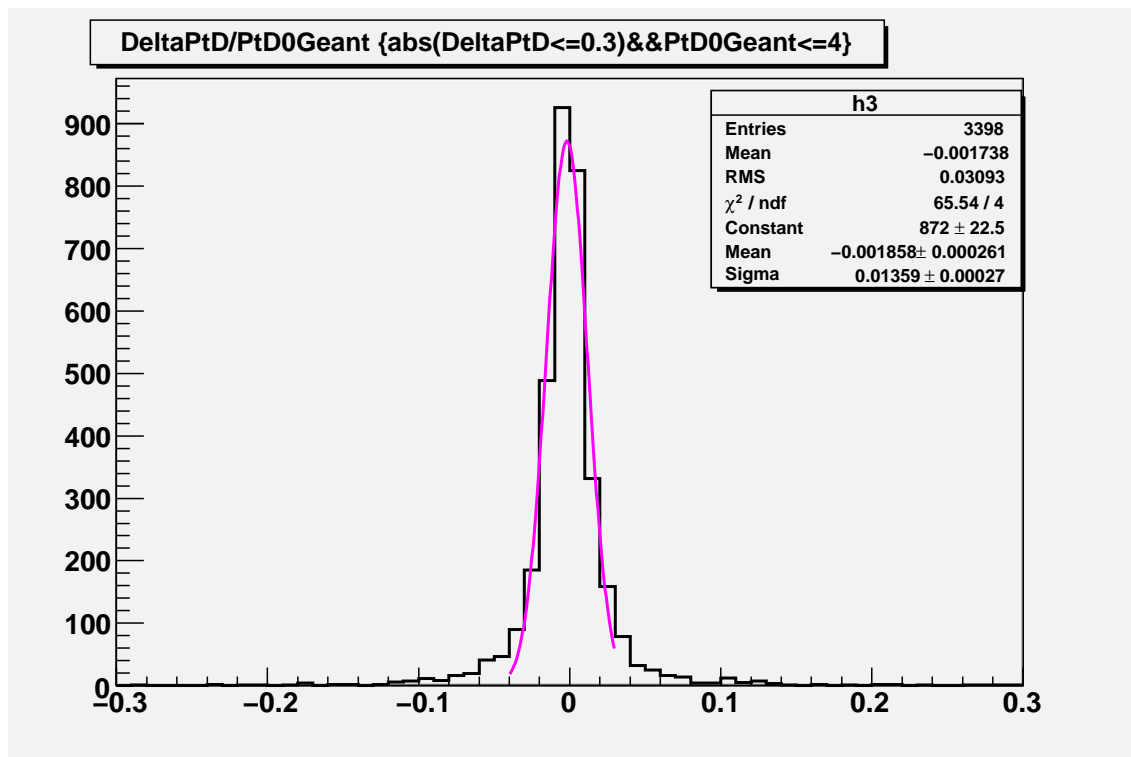


Figure 3.12: The percentage resolution of the $D^0 p_T$ fitted with a Gaussian curve (pink). The y-axis depicts the number of counts at the percentage.

curve with a Gaussian function (shown in pink) and the resulting σ is about 1 percent, which is compatible with expectations from the experimental resolution of the apparatus. Further correlations of these variables among themselves and also with other variables should allow for smarter cuts to be developed.

Chapter 4

Summary

In this thesis we performed an initial study of cut variables that will help improve the signal to background ratio while reconstructing D^0 -meson decays. Let us remember that we initiated this study for the first time here and therefore our scope of work is limited to lay down the foundation for further studies. We developed/debugged and tested the programming tools that allow for these variables to be correlated and studied in detail. We set up macros in the ROOT analysis environment that allowed us to analyze and graph these distributions. All this work was performed in an analysis environment with which we were completely unfamiliar, using programming languages like C++ on data sets that contained extremely complex information. This was not an easy task but our satisfaction comes from knowing that these tools are going to be well used in the study of charmed mesons, which will enhance our understanding of nuclear collisions and the world around us.

References

- [1] A. Liddle. *An Introduction to Modern Cosmology*. John Wiley and Sons, 2007.
- [2] C. Chasman et al. A heavy flavor tracker for star, 2008.
- [3] RHIC Website. <http://www.bnl.gov/rhic/>, 2008.
- [4] F. Bergsma et al. The star detector magnet subsystem. *Nucl. Instr. and Meth. A*, 499, 2003.
- [5] J. M. Landgraf et al. An overview of the star daq system. *Nucl. Instr. and Meth. A*, 499, 2003.
- [6] M. Andersen et al. The star time projection chamber: A unique tool for studying high multiplicity events at rhic. *Nucl. Instr. and Meth. A*, 499, 2003.
- [7] R. Bellwied et al. The star silicon vertex tracker: A large area silicon drift detector. *Nucl. Instr. and Meth. A*, 499, 2003.
- [8] B. E. Norman. *High P_T Charged Kaon Production in $\sqrt{s_{NN}} = 200\text{GeV}$ Au-Au Collisions at RHIC*. PhD thesis, Kent State University, 2003.
- [9] X. N. Wang. <http://www-nsdth.lbl.gov/xnwang/hijing/>, 1997.
- [10] J. Apostolakis. <http://wwwasd.web.cern.ch/wwwasd/geant/>, 2003.